

# Thresholdless Transition to Coherent Emission at Telecom Wavelengths from Coaxial Nanolasers with Excitation Power Dependent $\beta$ -Factors

Sören Kreinberg, Kaisa Laiho, Frederik Lohof, William E. Hayenga, Pawel Holewa, Christopher Gies, Mercedeh Khajavikhan, and Stephan Reitzenstein\*

The ongoing miniaturization of semiconductor lasers has enabled ultra-low threshold devices and even provided a path to approach thresholdless lasing with linear input–output characteristics. Such nanoscale lasers have initiated a discourse on the origin of the physical mechanisms involved and their boundaries, such as the required photon number, the importance of optimized light confinement in a resonator, and mode-density enhancement. Here, high- $\beta$  metal-clad coaxial nanolasers, which facilitate thresholdless lasing are investigated. Both the conventional lasing characteristics, as well as the photon statistics of the emitted light at 10 K under continuous wave excitation are experimentally and theoretically investigated. While the former lacks adequate information to determine the threshold to coherent radiation, the latter reveals a finite threshold pump power. The work confirms an important aspect of high- $\beta$  lasers, namely that a thresholdless laser does have a finite threshold pump power and must not be confused with a hypothetical zero-threshold laser. Moreover, the results reveal an excitation power dependent  $\beta$ -factor which needs to be taken into account to correctly describe the experimental data.

The properties and the terminology of thresholdless lasing have accompanied the development of laser physics in the last decades. More recently, the realization of nanoscale devices operating in the thresholdless regime have brought these issues to the forefront of science and technology. Nanolasers manifesting linear input–output characteristics in a double-logarithmic scale are usually referred to as thresholdless lasers,<sup>[1]</sup> in which case all the spontaneously generated photons are emitted into the lasing mode ( $\beta = 1$ ). The disappearance of the intensity jump is a consequence of the absence of radiative and non-radiative emission losses in high- $\beta$  lasers. However, the term thresholdless, which refers to a linear input–output characteristics, is somewhat ambiguous, as such lasers may wrongly be understood to exhibit a zero threshold pump power. To resolve this issue, it is paramount to identify

the excitation level at which the onset of the stimulated emission occurs via quantum optical studies. The autocorrelation function is the measurement of choice, as it reveals a distinctive change from chaotic to Poissonian photon statistics when coherent emission is reached. When dealing with high- $\beta$  nanolasers, one needs to carefully assess both the emission intensity and the statistical properties of the emitted light, as has been pointed out in the demonstration of nanolasers operating with different gain materials and cavity designs.<sup>[2–5]</sup> This is also of relevance for a new generation of nanolasers using monolayer flakes of semiconducting transition-metal dichalcogenides (TMDs) as gain material (see, e.g., refs. [6–9]).

Thresholdless input–output curves have been observed in metallic coaxial nanolasers (CNLs) with InGaAsP quantum wells (QWs) as active material.<sup>[10,11]</sup> These structures emit radiation at telecommunication wavelengths and offer high potential for applications in silicon photonics and integrated optics.<sup>[12,13]</sup> In particular, they can be fabricated with outer diameters of only a few hundred nanometers, resulting in ultra-small footprints. The possible observation of thresholdless lasing in QW systems brings about a debate as to whether these devices are indeed lasers capable of generating coherent radiation. In addition, it opens up a course of discussions on the role of various

Dr. S. Kreinberg, Dr. K. Laiho<sup>[+]</sup>, P. Holewa, Prof. S. Reitzenstein  
Institut für Festkörperphysik  
Technische Universität Berlin  
Hardenbergstr. 36, 10623 Berlin, Germany  
E-mail: stephan.reitzenstein@physik.tu-berlin.de

Dr. F. Lohof, Dr. C. Gies  
Institut für Theoretische Physik  
Universität Bremen  
Otto-Hahn-Allee 1, 28359 Bremen, Germany

Dr. W. E. Hayenga, Prof. M. Khajavikhan  
CREOL  
The College of Optics and Photonics  
University of Central Florida  
Orlando, FL 32816-2700, USA

 The ORCID identification number(s) for the author(s) of this article can be found under <https://doi.org/10.1002/lpor.202000065>

[+]Present address: Institute of Quantum Technologies, German Aerospace Center (DLR), Söflinger Straße 100, D-89077 Ulm, Germany

© 2020 The Authors. Laser & Photonics Reviews published by Wiley-VCH GmbH. This is an open access article under the terms of the Creative Commons Attribution License, which permits use, distribution and reproduction in any medium, provided the original work is properly cited.

DOI: 10.1002/lpor.202000065

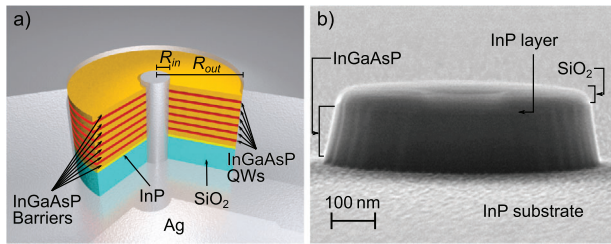


**Figure 1.** a) Cut-away schematic of a metallic coaxial nanolaser. b) Scanning electron microscope image (SEM) of the dielectric filling of a CNL after dry etching, before silver deposition. After silver deposition, the sample is flipped and the InP substrate is etched away. A 10 nm capping layer of InP covers the InGaAsP region. The ends of the active medium are terminated by a 100 nm high SiO<sub>2</sub> plug on one side and a 20 nm high vacuum plug on the other, which provides an avenue to pump the devices and to also outcouple the generated radiation. Details on the fabrication can be found in the Supporting Information.

physical mechanisms required to ensure operation in this regime.

In this work, we study the power dependent second-order coherence for two metallic nanolasers, one of which shows operation very close to the thresholdless lasing regime associated with a  $\beta$ -factor of 0.9 and negligible non-radiative loss rate. For this purpose, we compare conventional signs of lasing to quantum-optical studies of the second-order autocorrelation function. Accompanying the experimental investigation, we employ a microscopic laser model to obtain important insight in the interplay of the CNL's properties and their effect on the photon statistics of the emission. Noteworthy, in contrast to conventional microlaser theories, in our description the  $\beta$ -factor does not play the role of a constant device-dependent parameter but is calculated directly from the spontaneous-emission (SE) rates of carriers in the band structure into lasing and non-lasing modes. We find the resulting  $\beta$ -factor to be an excitation-power dependent parameter due to phase-space filling effects. Additionally, we show that special care has to be taken when investigating the second-order correlation function of nanolasers by using narrow-band spectral filtering. Indeed, in our case it results in an enhanced intensity noise resulting in pseudo-thermal characteristics, which can cause pitfalls in the interpretation of the emitted light.<sup>[14,15]</sup> Importantly, the previous studies of nanolasers with close-to thresholdless behavior do show the existence of a finite threshold, reconfirming that thresholdless lasing should not be confused as lasing with a zero threshold pump power.<sup>[16–19]</sup> In fact, while near thresholdless operation has even been achieved at room temperature in the presence of significant non-radiative losses,<sup>[20]</sup> the latter could only be achieved in a hypothetical cavity subject to no losses.

The investigated coaxial nanolasers are depicted in **Figure 1**. The active medium in these cavities comprises a ring of six InGaAsP QWs with an overall height of 200 nm radially sandwiched between an inner silver core with a radius of  $R_{in}$  and an outer metallic cladding confining the active medium to a radius of  $R_{out}$ . The two CNLs under study share a similar geometry, differing only in their inner and outer radii. This mainly alters the spectral locations of the supported modes and, in return, also the effective  $\beta$ -factor. The QWs result in a broad gain spectrum that spreads over several tens of nanometers close to the telecom E-

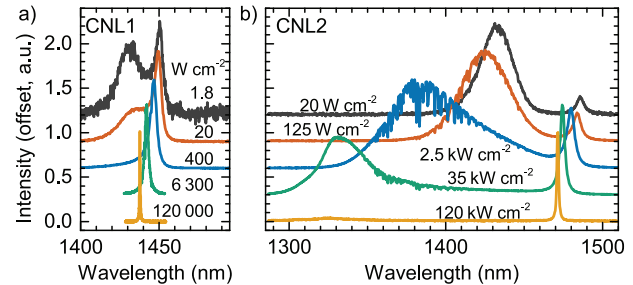


**Figure 2.** Excitation intensity-dependent  $\mu$ -PL spectra for CNL1 (panel a) and CNL2 (panel b). At low excitation intensities, a broad non-lasing spectral peak is found at smaller detuning for CNL1 ( $\delta\lambda = 20$  nm) than for CNL2 ( $\delta\lambda = 53$  nm). In all spectra, the height of the most prominent peak is normalized to unity. Due to absorption in humid air, distortion is apparent in some spectra. The broad emission feature observed for both CNLs in the shorter wavelengths is associated with the TM<sub>01</sub>-like mode. The gain maximum is centered at about 1430 nm and shows only a slight dependence of the excitation intensity (see Figure S7, Supporting Information).

and S-bands at cryogenic temperatures. We label the investigated structures with CNL1 ( $R_{out}$ : 295 nm,  $R_{in}$ : 55 nm) and CNL2 ( $R_{out}$ : 315 nm,  $R_{in}$ : 75 nm). In both cases, the azimuthally polarized TE<sub>01</sub>-like mode, exhibiting the largest quality factor and highest confinement factor, is expected to lase. The mode structure and the Q-factors were determined by numerical simulations using the finite elements method approach as detailed in the Supporting Information. For the calculations, we considered the geometry and material properties, such as the low temperature relative permittivity, of the nanolasers. Because experimentally determined values of silver's permittivity at 1.5  $\mu$ m wavelength and at low temperature are not available, we approximated the permittivity based on values reported in refs. [21–23] to obtain best global agreement between our experimental nanolaser data and the predictions of our microscopic laser theory. The chosen value of  $\epsilon_{Ag} = -126 - i0.300$  leads to Q-factors of  $Q = 1030$  for CNL1 and  $Q = 815$  for CNL2 which are consistent with the experimental data presented in Figure 3g,h in the sense that they correspond to emission linewidths of 1.4 nm (CNL1) and 1.8 nm (CNL2) at excitation intensities slightly below the laser threshold where absorption by the gain medium is nearly quenched and linewidth narrowing due to the onset of coherence is not yet significant. To underline the suitability of this approximation, we performed additional contrasting simulations using a permittivity with a higher imaginary part of  $\epsilon_{Ag} = -103 - i1.300$  and  $\epsilon_{Ag} = -108 - i1.4$  which are obtained, for instance, by a simple extrapolation of the short wavelength values reported in ref. [24] to the wavelengths of CNL1 and CNL2. The different permittivity leads to significantly lower Q-factors of  $Q = 510$  for CNL1 and  $Q = 430$  for CNL2. These values are less compatible with the experimental linewidths presented in Figure 3g,h as they correspond to the values of 2.9 nm (CNL1) and 3.5 nm (CNL2) at excitation intensities where the absorption by the gain medium is dominating (whereas the theory considers Q-factors at transparency, i.e., in the absence of quantum well absorption). Using these alternative Q-factors, we are not able to describe the experimental data in a consistent way by our microscopic laser theory.

Preliminary information about laser action in the CNLs is obtained by excitation-intensity dependent  $\mu$ -PL studies under CW

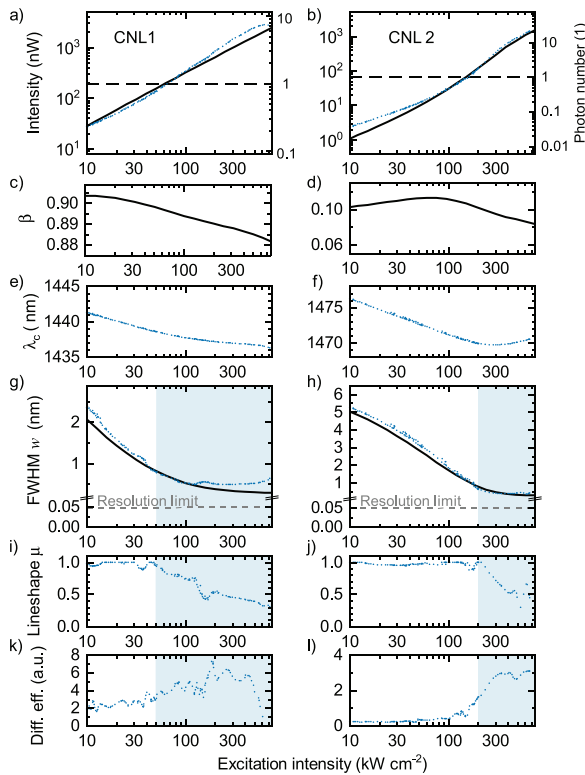


**Figure 3.** Excitation power dependent optical properties of the CNLs: a,b) Integrated emission intensity and intra-cavity photon number; c,d)  $\beta$ -factor, e,f) central emission wavelength  $\lambda_c$ , g,h) spectral full width at half maximum (FWHM)  $\omega$ , i,j) lineshape parameter  $\mu$ , and k,l) differential efficiency for CNL1 (left) and CNL2 (right). Measured values are illustrated with symbols, whereas the black solid lines are predicted by the theoretical model (see Supporting Information). The dashed lines in (a,b) indicate a mean intra-cavity photon number of one, which is often regarded as a threshold condition for nanolasers.<sup>[1,30]</sup> CNL1 and CNL2 meet this criterion at pump rates of approximately 65 and 155 kW cm<sup>-2</sup>, respectively. We note that the azimuthally polarized light from the CNLs is projected to a linear polarization prior to measurement. The wiggling artifacts are caused by absorption of the CNL emission in humid air.

excitation at 10 K, where non-radiative losses have minor impact. The experimental setup used for our investigations is introduced in the Supporting Information. A selection of the measured spectra is presented in **Figure 2** for both CNLs. To extract the conventional laser characteristics, which are shown in **Figure 3**, the measured  $\mu$ -PL spectra are fitted with pseudo-Voigt profiles (see Supporting Information). While the integrated mode intensity of CNL1 (**Figure 3a**) features a nearly linear input–output curve resembling thresholdless lasing, that of CNL2 (**Figure 3b**) shows a more prominent S-shape indicating a reduced  $\beta$ -factor. The experimental input–output curves agree well with our quantum-optical laser model (solid black curves in **Figure 3**) which is described in the Supporting Information. Slight deviations from the S-shape of CNL2 may be explained by the possible contribution of zero-dimensional gain centers at low excitation<sup>[4]</sup> not captured by a description based solely on a 2D QW gain medium.

Spontaneous and stimulated emission into the laser mode result from the steady-state occupation of carrier states in the

band structure. For our laser model, the light–matter coupling constants for both CNLs are determined by matching the measured and calculated cavity-enhanced time-resolved photoluminescence (TRPL) traces (see **Figure S4**, Supporting Information). Radiative losses enter in the form of an effective rate, which then allows us to calculate the  $\beta$ -factor (see Equation (S24), Supporting Information). As shown in **Figure 3c,d** it exhibits a decrease with increasing excitation power. The origin of the observed excitation-power-induced change of the  $\beta$ -factor is attributed to the non-equilibrium carrier-distribution functions that enter the SE rate and, thereby influence  $\beta$ . At the onset of stimulated emission, we observe hole burning in the carrier distribution functions in the spectral vicinity of the cavity resonance and the SE rate into the laser mode no longer grows. At the same time, with increasing excitation power, populations still rise in parts of the band structure that are not depleted by stimulated emission into the laser mode. The increasing number of carriers in higher-lying states leads to a larger SE into the non-lasing modes, which in effect lowers the  $\beta$ -factor (see Supporting Information). The peak value of  $\beta$  is reached at the point of the maximum SE rate into the laser mode in relation to radiative losses. The higher values of  $\beta$  with a maximum of 0.9 obtained for CNL1 are consistent with its practically thresholdless behavior. In CNLs, the high  $\beta$ -factor stems from a strong light–matter interaction leading to an enhancement of radiative decay.<sup>[11]</sup> To support this explanation, we discuss the excitation-power dependence of  $\beta$  in the Supporting Information in more detail. In this context, we present TRPL lifetime measurements and calculations for both CNLs and compare these with the lifetime in planar material, from which a Purcell factor of about 15 is estimated. Noteworthy, the corresponding lifetimes were extracted at excitation powers well below the laser threshold to avoid a possible influence of stimulated emission on determining the Purcell factor.<sup>[25]</sup> Other factors have been identified to modify the SE rate and the  $\beta$ -factor at constant excitation power, such as line-shape effects and spectral detuning,<sup>[26,27]</sup> even in the presence of fast dephasing,<sup>[28]</sup> as well as population effects.<sup>[29]</sup>

A closer inspection of the spectral characteristics of the CNLs is required to access other conventional signs of lasing. **Figure 3e,f** reveal that the central wavelengths of both CNLs show strong blue-shifting with respect to the growing excitation intensity. However, at higher intensities, CNL2's emission wavelength experiences red-shifting, which is attributed to heating effects. Additionally, both CNLs show linewidth narrowing by about one order of magnitude for the excited mode within the measured intensity range, which is in agreement with the calculations presented in **Figure 3g,h**. At high excitation densities, we expect that thermally induced gain changes are transformed into fluctuations in the resonant wavelength due to the Kramers–Kronig relations (see, e.g., ref. [31]). This can explain the saturation, and even slight increase for CNL1, of the emission linewidth at excitation intensities exceeding about 200 kW cm<sup>-2</sup>. Within the investigated range of excitation intensities the spectral lineshapes change from a Lorentzian to Gaussian profile, which is reflected in the Pseudo-Voigt profile by  $\mu$  changing from 1 to about 0.3 (see Supporting Information) in **Figure 3i,j**. Interestingly, this change begins at the same excitation intensities at which the emission linewidth starts to saturate, that is around 50 kW cm<sup>-2</sup> for CNL1 and around 200 kW cm<sup>-2</sup> for CNL2, possibly indicating the onset

of temperature induced inhomogeneous broadening at higher excitation intensities. While such thermal effects are not included in the modeling, the key saturation feature of the linewidth reduction is reproduced irrespective of the spectral lineshape. From the linewidths, coherence times can be obtained, and we estimate a lower limit of 0.3 ps below threshold to 8 ps above threshold (see Supporting Information). The obtained picture is complemented by the differential efficiency plotted in Figure 3k,l for the two nanolasers. In case of CNL2 with a moderate  $\beta$ -factor, the transition to stimulated emission is reflected in a pronounced increase of the differential efficiency at around  $200 \text{ kW cm}^{-2}$ . In contrast, for the high- $\beta$  laser CNL1, such a clear feature is absent which underlines the need for quantum-optical studies to understand the threshold behavior of high- $\beta$  lasers in full detail.

Recently, we showed that an almost linear input–output characteristic accompanied by linewidth narrowing can occur in the regime of amplified SE, which can be identified by assessing the photon statistics of the associated emission.<sup>[32]</sup> To rule out this possibility in the case of CNL1 and to estimate the threshold pump density, we study the time-dependent second-order autocorrelation function  $g^{(2)}(\tau)$  (see Supporting Information for details on the measurement) by selecting the CNLs' mode via a 12 nm bandpass filter. In Figure 4a,b, we present two of the measured coincidence histograms  $g^{(2)}(\tau)$  for CNL1. We extract raw values of  $g^{(2)}(0)$  by fitting Gaussian temporal profiles to the measured data. The fitted peak heights are presented in Figure 4c,d for both CNLs showing gradually decreasing  $g^{(2)}(0)$  at excitation intensities higher than about  $100 \text{ kW cm}^{-2}$ . Below that, the raw values of  $g^{(2)}(0)$  are more strongly limited by the temporal resolution of our  $g^{(2)}(\tau)$ -setup due to the excitation-power dependent coherence time.<sup>[2,33]</sup> The raw measured  $g^{(2)}(\tau)$  histograms are then deconvoluted, compensating for the finite timing-jitter (50 ps) of our superconducting nanowire single-photon detectors following the procedure introduced in ref. [32] (see Supporting Information). In Figure 4e,f, we present the deconvoluted  $g_{\text{deconv}}^{(2)}(0)$  values for the investigated CNLs, which agree well with our theoretical prediction. As expected, for high- $\beta$  lasers the threshold region is smeared out, but from the autocorrelation measurements we can conclude that the transition toward coherent emission occurs at about  $30\text{--}100 \text{ kW cm}^{-2}$  ( $150\text{--}300 \text{ kW cm}^{-2}$ ) for CNL1 (CNL2).

Moreover, we perform a second series of excitation-intensity dependent measurements of  $g^{(2)}(\tau)$  for CNL1 with tight spectral filtering as shown in Figure 4e with red squares (see Supporting Information). The effect of narrowband spectral filtering in the HBT measurement is of particular relevance when studying the emission of nanolasers, which often have small cavity quality factors and large emission linewidths. In our case, a too narrow spectral selection in  $g^{(2)}(\tau)$ -setup leads to artifacts in the associated photon autocorrelation and an incorrect interpretation of the measured autocorrelation function.

Altogether, the good agreement between experiment and theory supports the validity of the simple and approximative deconvolution procedure performed on the raw  $g^{(2)}(0)$  data from our CNLs. More generally, in the regime where cavity-QED effects dominate the emission dynamics, the autocorrelation function may be modified in ways that render the Siegert relation unsuited for extrapolating, as we discuss in the Supporting Information. However, the suitability of our approach is supported by the fact that the raw data is reproduced by theory if the calculated coher-

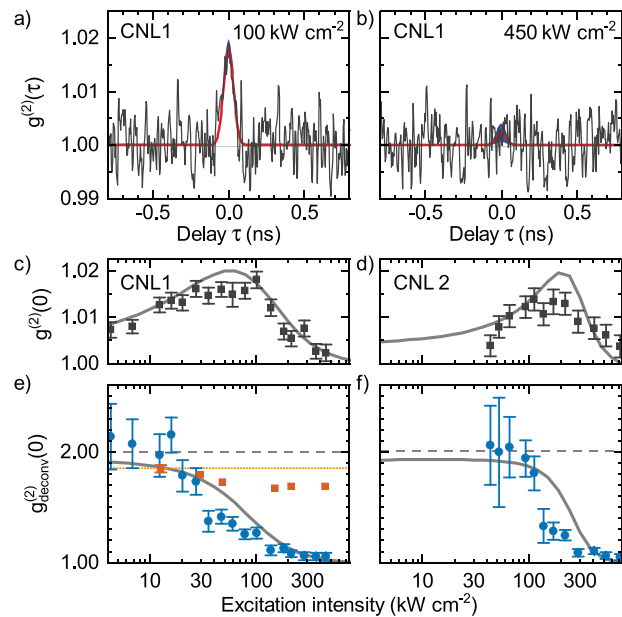


**Figure 4.** a,b) Experimental  $g^{(2)}(\tau)$  coincidence histograms (black lines) for CNL1 measured at different excitation intensities, together with the Gaussian fits (red lines, uncertainties blue) yielding  $g^{(2)}(0) = 1.0180 \pm 0.0018$  and  $1.0023 \pm 0.0018$ , respectively. The temporal resolution of our HBT setup is about 80 ps corresponding to the FWHM of the measured correlogram in a). c,d) Raw (black squares) and e,f) deconvoluted  $g^{(2)}(0)$  values (blue circles) for CNL1 (left) and CNL2 (right) with respect to excitation intensity. The raw values in (c,d) fit well with the theoretical predictions (gray solid lines) in (e,f) after being convoluted with the estimated  $g^{(2)}(\tau)$ -setup response time (see Supporting Information). The red squares in (e) are raw values measured with narrow-band spectral filtering. As a validation of our setup, the orange dashed line shows the value of  $g^{(2)}(0)$  measured for a spectrally filtered incandescent lamp, for which thermal characteristics is expected by definition. The gray dashed line provides a guide for the eye.

ence times and the time resolution of the  $g^{(2)}(\tau)$ -setup are used to convolute the calculated result, producing the solid lines in Figure 4c,d. We emphasize that these predicted lines are not obtained from a fit, but result from calculated coherence times and  $g^{(2)}(0)$  for a single consistent parameter set for each CNL (see Supporting Information). Clearly, both the experiment and theory provide strong evidence for a transition from spontaneous to stimulated emission and indicate laser operation in both CNLs.

In conclusion, our combined experimental and theoretical quantum-optical investigations of metal-clad coaxial nanolasers provide unambiguous evidence for thresholdless laser operation with coherent emission at telecom wavelengths. The validity of the first- and second-order coherence properties obtained from experiment is supported by quantum-optical modeling, which yields simultaneous agreement of the input–output characteristics, coherence time, and autocorrelation function. From the microscopic laser model, we obtain a  $\beta$ -factor that is pump-power dependent in contrast to the wide-spread assumption of a device-dependent constant  $\beta$ . Our results highlight that it is crucial to collect the spectrally broad emission line of a nanolaser without truncating its spectral tails in order to correctly access the underlying photon statistics. As such, this work provides the first comprehensive characterization of thresholdless lasing in high- $\beta$

metallic quantum-well nanoscale lasers. It paves the way for designing the next generation of ultrasmall coherent light sources, benefiting from quantum effects appearing at the nanoscale.

## Supporting Information

Supporting Information is available from the Wiley Online Library or from the author.

## Acknowledgements

The research leading to these results has received funding from the European Research Council (ERC) under the European Union's Seventh Framework ERC Grant Agreement No. 615613. K.L. acknowledges support from the Austrian Science Fund (FWF): J-4125-N27. C.G. and F.L. acknowledge funding from the Deutsche Forschungsgemeinschaft (DFG) via the graduate school "Quantum-Mechanical Material Modeling" GRK 2247/1-1. The authors thank Marcel Hohn, Nicole Srocka, and Tobias Heindel for laboratory support.

Open access funding enabled and organized by Projekt DEAL.

## Conflict of Interest

The authors declare no conflict of interest.

## Keywords

microscopic theory, nanolasers, photon statistics, quantum wells, thresholdless lasing

Received: February 25, 2020

Revised: September 29, 2020

Published online: November 8, 2020

- [1] G. Björk, A. Karlsson, Y. Yamamoto, *Phys. Rev. A* **1994**, *50*, 1675.
- [2] S. Strauf, K. Hennessy, M. T. Rakher, Y. S. Choi, A. Badolato, L. C. Andreani, E. L. Hu, P. M. Petroff, D. Bouwmeester, *Phys. Rev. Lett.* **2006**, *96*, 127404.
- [3] J. Wiersig, C. Gies, F. Jahnke, M. Aßmann, T. Berstermann, M. Bayer, C. Kistner, S. Reitzenstein, C. Schneider, S. Höfling, A. Forchel, C. Kruse, J. Kalden, D. Hommel, *Nature* **2009**, *460*, 245.
- [4] S. T. Jagsch, N. V. Triviño, F. Lohof, G. Callsen, S. Kalinowski, I. M. Rousseau, R. Barzel, J. F. Carlin, F. Jahnke, R. Butté, C. Gies, A. Hoffmann, N. Grandjean, S. Reitzenstein, *Nat. Commun.* **2018**, *9*, 564.
- [5] W. W. Chow, S. Reitzenstein, *Appl. Phys. Rev.* **2018**, *5*, 041302.
- [6] S. Wu, S. Buckley, J. R. Schaibley, L. Feng, J. Yan, D. G. Mandrus, F. Hatami, W. Yao, J. Vuckovic, A. Majumdar, X. Xu, *Nature* **2015**, *520*, 69.
- [7] Y. Ye, Z. J. Wong, X. Lu, X. Ni, H. Zhu, X. Chen, Y. Wang, X. Zhang, *Nat. Photon.* **2015**, *9*, 733.
- [8] C. Javerzac-Galy, A. Kumar, R. D. Schilling, N. Piro, S. Khorasani, M. Barbone, I. Goykhman, J. B. Khurgin, A. C. Ferrari, T. J. Kippenberg, *Nano Lett.* **2018**, *18*, 3138.
- [9] F. Lohof, R. Barzel, P. Gartner, C. Gies, *Phys. Rev. Appl.* **2018**, *10*, 054055.
- [10] M. Khajavikhan, A. Simic, M. Katz, J. H. Lee, B. Slutsky, A. Mizrahi, V. Lomakin, Y. Fainman, *Nature* **2012**, *482*, 204.
- [11] W. E. Hayenga, H. Garcia-Gracia, H. Hodaie, Y. Fainman, M. Khajavikhan, *Adv. Phys. X* **2016**, *1*, 262.
- [12] R. Chen, T. T. D. Tran, K. W. Ng, W. S. Ko, L. C. Chuang, F. G. Sedgwick, C. Chang-Hasnain, *Nat. Photon.* **2011**, *5*, 170.
- [13] S. Zhu, B. Shi, Q. Li, K. M. Lau, *Opt. Express* **2018**, *26*, 14514.
- [14] R. C. Neelen, D. M. Boersma, M. P. van Exter, G. Nienhuis, J. P. Wordman, *Phys. Rev. Lett.* **1992**, *69*, 593.
- [15] R. C. Neelen, D. M. Boersma, M. P. van Exter, G. Nienhuis, J. P. Wordman, *Opt. Commun.* **1993**, *100*, 289.
- [16] E. Yablonovitch, *Phys. Rev. Lett.* **1987**, *58*, 2059.
- [17] F. De Martini, G. R. Jacobovitz, *Phys. Rev. Lett.* **1988**, *60*, 1711.
- [18] S. Noda, *Science* **2006**, *314*, 260.
- [19] A. A. Vyshnevyy, D. Y. Fedyanin, *Opt. Express* **2018**, *26*, 33473.
- [20] I. Prieto, J. M. Llorens, L. E. Muñoz-Camuniez, A. G. Taboada, J. Canet-Ferrer, J. M. Ripalda, C. Robles, G. Muñoz-Matutano, J. P. Martínez-Pastor, P. A. Postigo, *Optica* **2015**, *2*, 66.
- [21] J. S. T. Smalley, M. W. Puckett, Y. Fainman, *Opt. Lett.* **2013**, *38*, 5161.
- [22] J. S. T. Smalley, Q. Gu, Y. Fainman, *IEEE J. Quantum Electron.* **2014**, *50*, 175.
- [23] Q. Gu, J. S. Smalley, J. Shane, O. Bondarenko, Y. Fainman, *Nanophotonics* **2015**, *4*, 26.
- [24] S. V. Jayanti, J. H. Park, A. Dejneka, D. Chvostova, K. M. McPeak, X. Chen, S. H. Oh, D. J. Norris, *Opt. Mater. Express* **2015**, *5*, 1147.
- [25] J. Canet-Ferrer, I. Prieto, G. Muñoz-Matutano, L. J. Martínez, L. E. Muñoz-Camuniez, J. M. Llorens, D. Fuster, B. Alén, Y. González, L. González, P. A. Postigo, J. P. Martínez-Pastor, *Appl. Phys. Lett.* **2013**, *102*, 201105.
- [26] M. Fujita, R. Ushigome, T. Baba, *IEEE Photonics Technol. Lett.* **2001**, *13*, 403.
- [27] D. Englund, D. Fattal, E. Waks, G. Solomon, B. Zhang, T. Nakaoka, Y. Arakawa, Y. Yamamoto, J. Vučković, *Phys. Rev. Lett.* **2005**, *95*, 013904.
- [28] H. Sumikura, E. Kuramochi, H. Taniyama, M. Notomi, *Phys. Rev. B* **2016**, *94*, 195314.
- [29] N. Gregersen, T. Suhr, M. Lorke, J. Mørk, *Appl. Phys. Lett.* **2012**, *100*, 131107.
- [30] L. Reeves, Y. Wang, T. F. Krauss, *Adv. Optical Mater.* **2018**, *6*, 1800272.
- [31] Y. Yamamoto, *Coherence, Amplification, and Quantum Effects in Semiconductor Lasers*, Wiley Series in Pure and Applied Optics, Wiley, New York **1991**.
- [32] S. Kreinberg, W. W. Chow, J. Wolters, C. Schneider, C. Gies, F. Jahnke, S. Höfling, M. Kamp, S. Reitzenstein, *Light Sci. Appl.* **2017**, *6*, e17030.
- [33] S. M. Ulrich, C. Gies, S. Ates, J. Wiersig, S. Reitzenstein, C. Hofmann, A. Löffler, A. Forchel, F. Jahnke, P. Michler, *Phys. Rev. Lett.* **2007**, *98*, 043906.